



# Fast peptide exchange on major histocompatibility complex class I molecules by acidic stabilization of a peptide-empty intermediate

Ankur Saikia<sup>1</sup>  | Andries Haderler<sup>1</sup> | Pranathi Prasad<sup>1</sup> | Martin Zacharias<sup>2</sup> | Sebastian Springer<sup>1</sup> 

<sup>1</sup>School of Science, Jacobs University Bremen, Bremen, Germany

<sup>2</sup>Physik-Department, T38, Technical University of Munich, Munich, Germany

## Correspondence

Sebastian Springer, School of Science, Jacobs University Bremen, Campus Ring 1, 28759 Bremen, Germany.  
Email: [s.springer@jacobs-university.de](mailto:s.springer@jacobs-university.de)

## Funding information

Deutsche Forschungsgemeinschaft, Grant/Award Number: SP583/12-1

**Review Editor:** John Kuriyan

## Abstract

The cell biology and biochemistry of peptide exchange on major histocompatibility complex class I (MHC-I) proteins are of great interest in the study of immunodominance, which requires iterative optimization of peptide affinity, and cross-presentation of pathogen and tumor antigens, in which endogenous peptides are exchanged for exogenous ones. Even though several methods exist to catalyze peptide exchange on recombinant MHC-I proteins, the cellular conditions and mechanisms allowing for peptide exchange in vivo remain unclear. Here, we demonstrate that low pH, as present in endosomes, indeed triggers peptide exchange, and we dissect the individual steps of the exchange reaction. We find that low pH stabilizes the peptide-empty forms of MHC-I that occur as intermediates of the exchange reaction, and that is synergizes with dipeptides and with disulfide-mediated stabilization of MHC-I.

## KEYWORDS

crosspresentation, fluorescence anisotropy, major histocompatibility complex class I molecules, peptide exchange

## 1 | INTRODUCTION

Major histocompatibility complex class I molecules (MHC-I) bind intracellular peptides in the endoplasmic reticulum (ER) and present them on the cell surface, allowing for immune surveillance by CD8<sup>+</sup> T cells.<sup>1</sup> Peptide loading onto MHC-I in the ER involves iterative

optimization, with low-affinity peptides exchanged for those with higher affinity, usually aided by the chaperones tapasin or TAPBPR (transporter associated with antigen processing binding protein-related).<sup>2–4</sup> Peptide exchange is also thought to be central to cross-presentation, where in the endocytic pathway of professional antigen-presenting cells, peptides previously loaded onto

**Abbreviations:** A2, human MHC-I allotype HLA-A\*02:01; A24, human MHC-I allotype HLA-A\*24:02; dsA2, disulfide-stabilized A2; dsA24, disulfide-stabilized A24; dsMHC-I, disulfide-stabilized MHC-I; ER, endoplasmic reticulum; MD, molecular dynamics; MHC-I, major histocompatibility complex class I molecule(s); nanoDSF, nanoscale differential scanning tryptophan fluorimetry; TAPBPR, transporter associated with antigen processing binding protein-related; wtA2, wild-type A2; wtA24, wild-type A24;  $\beta_2m$ , beta-2 microglobulin.

Classification: Biological Sciences/Immunology and Inflammation (or Biochemistry).

This is an open access article under the terms of the [Creative Commons Attribution-NonCommercial](https://creativecommons.org/licenses/by-nc/4.0/) License, which permits use, distribution and reproduction in any medium, provided the original work is properly cited and is not used for commercial purposes.

© 2022 The Authors. *Protein Science* published by Wiley Periodicals LLC on behalf of The Protein Society.

MHC-I are replaced by exogenous peptides in order to activate cytotoxic T cells against tumors.<sup>5</sup> The molecular mechanisms and cellular conditions mediating peptide exchange, especially in the absence of exchange chaperones (as occurs in tumors that downregulate them), with tapasin-independent allotypes, and during cross-presentation, are not well understood. Of key interest is the role of pH, since the low pH of endocytic compartments has been postulated to destabilize the peptide-MHC-I complex to enhance peptide exchange during cross-presentation.<sup>6,7</sup>

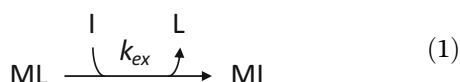
Peptide exchange on recombinant MHC-I is also of technological interest since they are used in the study of antigen-specific CD8<sup>+</sup> T cell populations. Peptide exchange allows for the rapid generation of large numbers of peptide-MHC-I complexes for the analysis of anti-tumor and antiviral immune responses and for safety screening of recombinant T cell receptors.<sup>8,9</sup>

We and others have identified several techniques for accelerating peptide exchange, among them the use of dipeptides that catalyze rapid peptide exchange at room temperature and pH 7.<sup>10–14</sup> Here, we show that acidic pH accelerates peptide exchange by stabilizing a peptide-free intermediate of the reaction.

## 2 | RESULTS

### 2.1 | Low pH accelerates peptide exchange on HLA-A\*02:01 and HLA-A\*24:02

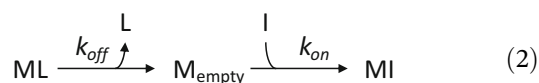
It has been previously proposed that low-affinity peptides are released from MHC-I at low pH values of 5.5 – 7 (corresponding to conditions in endolysosomal compartments) and exchanged for high-affinity peptides.<sup>7,15</sup> To test this proposition with recombinant proteins, we expressed the human MHC-I heavy chains HLA-A\*02:01 (in the following termed A2) and HLA-A\*24:02 (A24) in *Escherichia coli* and folded them in vitro with their light chain beta-2 microglobulin ( $\beta_2m$ ) and various low- and high-affinity peptides<sup>16</sup> (see Table S3 for a list of peptides). First, to validate the experimental system for monitoring peptide exchange, we used an established exchange technology, that is, dipeptide-catalyzed peptide exchange,<sup>11,17</sup> where the complex of MHC-I with a “leaving” peptide is incubated with an excess of “incoming” peptide and a high concentration of catalytic dipeptide, leading to peptide exchange. We monitored exchange by fluorescence anisotropy (Figure 1a,b), which measures the exchange rate constant ( $k_{ex}$ ):



(with M = MHC-I, L = leaving peptide, I = incoming peptide). Next, without dipeptide, we tested different pH values. Lowering the pH from 8 to 6 triggered a dramatic increase in the exchange rate for both allotypes, with up to 100-fold acceleration (Figure 1c–f, Table S1). Decreasing the pH any further was not feasible, since at pH 5.5,  $\beta_2m$  dissociates from the heavy chain.<sup>18</sup>

### 2.2 | Small effects of low pH on peptide association

To address the mechanistic details of this acidic acceleration of peptide exchange, we first assumed that peptide exchange consists of two steps, that is, the dissociation of the pre-bound (“leaving”) peptide, described by the dissociation rate constant  $k_{off}$ , and the association of the incoming peptide, described by the association rate constant,  $k_{on}$ , as follows:



Measuring the  $k_{on}$  separately from the  $k_{off}$  requires an empty receptor, and since the binding site of empty wild type MHC-I is natively unfolded and binds peptide only slowly (if at all),<sup>19–25</sup> we used empty disulfide-stabilized MHC-I (dsMHC-I) molecules, which have a disulfide bond linking the  $\alpha_1$  and  $\alpha_2$  helices of the peptide-binding groove, conformationally stabilizing the F pocket region in the absence of peptide in a structure that is close to the peptide-bound state.<sup>8,9,26–28</sup> We first validated the use of dsA2 and dsA24 by repeating the exchange experiments, and we found that they exchange peptides significantly faster than their wild type (wt) counterparts and that they, importantly, show a similar dipeptide-mediated and acidic acceleration of peptide exchange (Figure S1; Table S1). Disulfide stabilization did not significantly alter the affinity of A2 toward peptides and dipeptides (Tables S1 and S2).

We now measured the association rates ( $k_{on}$ ) of the fluorescently labeled peptides to the empty dsA2 and dsA24 molecules. Due to the very high association rate of peptide to dsA24, the data have limited value for that allotype; but for A2, decreasing the pH from 8 to 7 only doubled the  $k_{on}$  (Figure 2a,b; Table S1, Figure S5); when the pH was lowered further, from 7 to 6, the  $k_{on}$  remained the same (dsA24) or even decreased (dsA2). These results suggest that the acidic acceleration of peptide exchange is not caused by an increase in the peptide association rate.

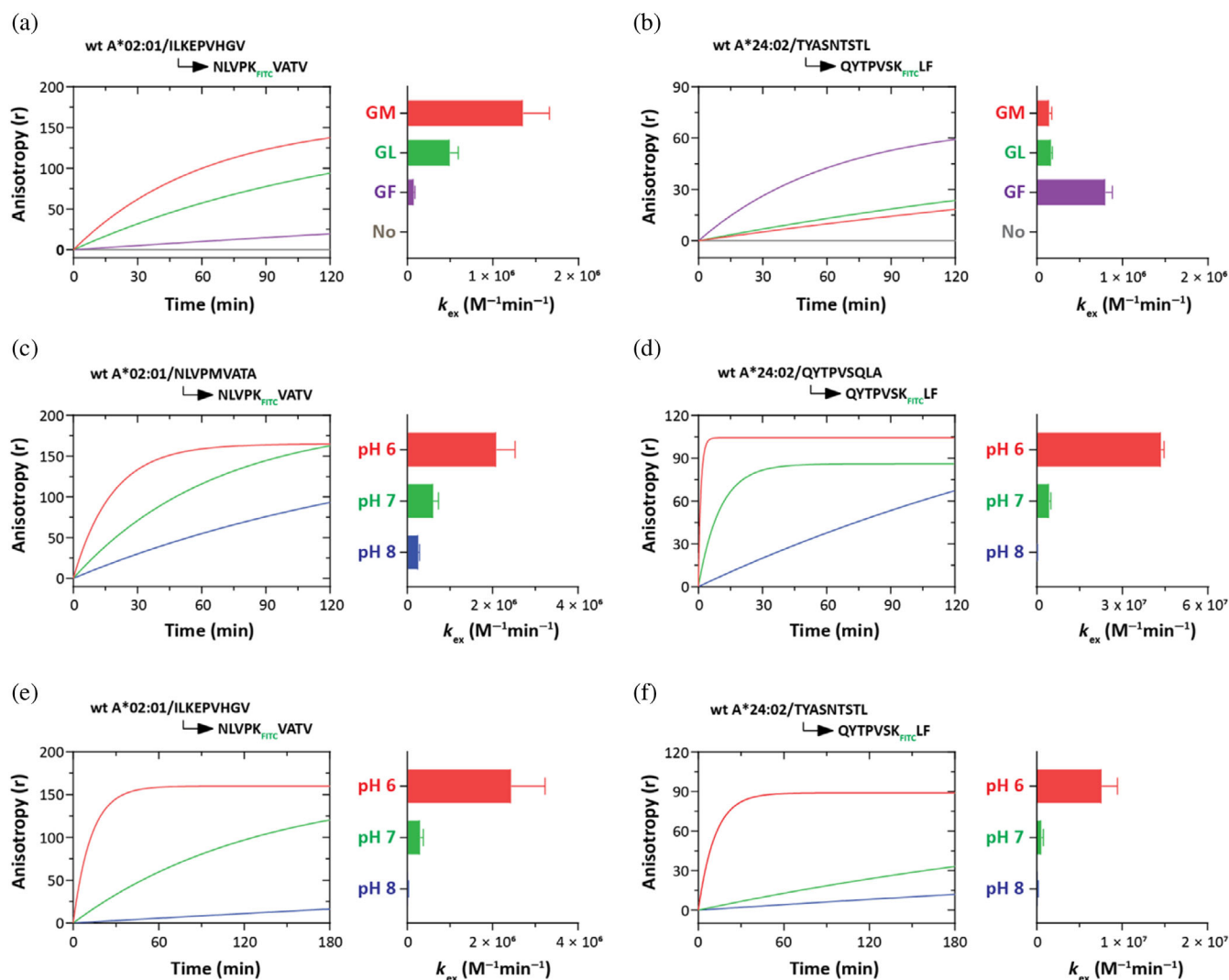


**FIGURE 1** Low pH promotes peptide exchange on wtA2 and wtA24. Peptide exchange was measured on A2 (a, c, e) and on A24 (b, d, f) by fluorescence anisotropy with MHC-I/peptide starting complexes (60 nM) and fluorescently labeled incoming peptides (20 nM) as indicated. Left panels show a representative experiment, right panels show averages of three experiments  $\pm$ SEM. (a and b) Dipeptide-mediated peptide exchange on A2 and A24 in 50 mM HEPES buffer and 100 mM NaCl at pH 7.5. (c and d) Exchange of low-affinity peptides at different pH values. (e and f) Exchange of high-affinity peptides at different pH values. Values and repeats are in Table S1.

### 2.3 | Small effects of low pH on peptide dissociation rate and equilibrium binding affinity

Therefore, we next sought to determine whether low pH destabilizes the complex of MHC-I with the leaving peptide, promoting peptide dissociation. First, we reasoned that an increased  $k_{off}$ , at a rather stable  $k_{on}$ , should be accompanied by an increase in the equilibrium dissociation constant ( $K_D$ ), since

$$K_D = \frac{k_{off}}{k_{on}}. \quad (3)$$

We, therefore, measured the  $K_D$  by peptide titration with steady-state anisotropy<sup>29</sup> and found that the pH did not

significantly affect the peptide binding affinity of the complexes (Figure 2c,d). Second, another readout of peptide binding affinity to MHC-I is the thermal stability of the peptide-MHC-I complexes<sup>20,30–35</sup>; to measure it, we used nanoscale differential scanning fluorimetry (nanoDSF), which quantifies protein unfolding by the change in the fluorescence emission of tryptophan indoles and generates a thermal denaturation curve, the midpoint of which corresponds to the melting temperature ( $T_m$ ).<sup>17</sup> We found that there was little influence of the pH on the  $T_m$  of high-affinity peptide complexes with wtA2 or wtA24, whereas for medium-affinity peptides, there was a slight stabilization at low pH (Figure 2e). Third, we directly measured the dissociation of a fluorescently labeled leaving peptide from dsA2 at different pH values and found a two-fold increased  $k_{off}$

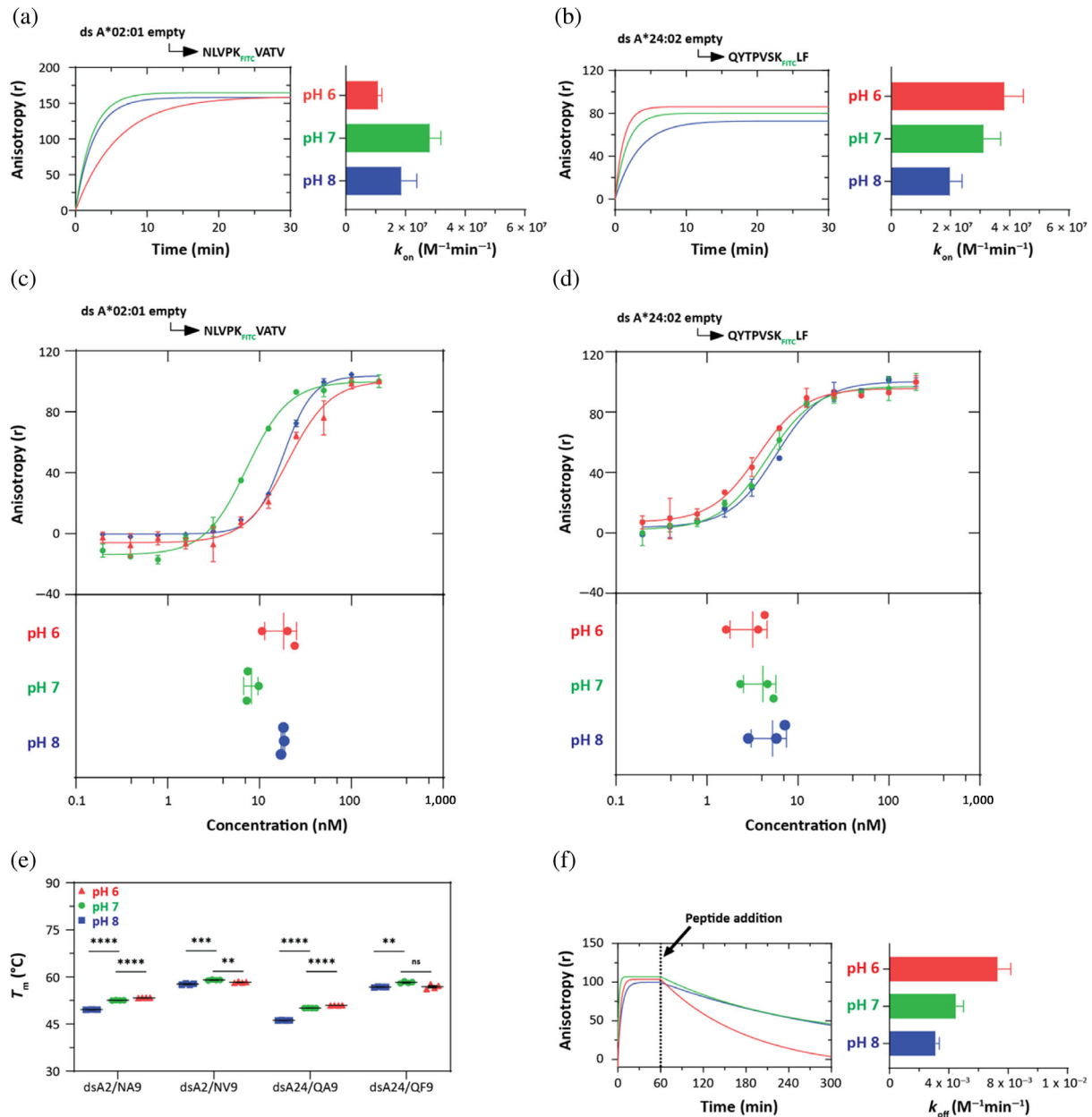


**FIGURE 2** Small effects of low pH on peptide association, dissociation, and complex stability. (a and b) Binding kinetics of FITC-labeled peptides onto 60 nM empty dsA2 and dsA24 in citrate-phosphate buffer at pH 6, 7, and 8. Association rate constants ( $k_{on}$ ) are shown in Table S1. (c and d) Equilibrium binding affinity of empty dsA2 and dsA24 measured by steady-state anisotropy with 2 nM FITC peptides (fixed concentration) titrated with 200–0.2 nM of the respective empty dsMHC-I, in citrate-phosphate buffer at pH 6, 7, and 8. (e) Thermostability of 100  $\mu$ g/ml ( $\sim$ 2.2  $\mu$ M) wtA2- and wtA24-peptide complexes in phosphate-buffered measured by nanoDSF. (f) Fluorescence anisotropy was used to track association of 10 nM NA9-TAM onto 30 nM empty dsA2, followed by dissociation after the addition of 10  $\mu$ M NV9 at 60 min. Full peptide sequences are shown in Table S4. Values and repeats are in Table S1 for kinetic and equilibrium measurements, and in Table S2 for thermostability.

at pH 6, compared to pH 8 and 7 (Figure 2f). Taken together, these data suggest that any pH-induced changes in the peptide dissociation rate or the peptide/MHC complex stability are subtle, and that they are not responsible for the strong acidic acceleration of peptide exchange.

## 2.4 | Small salt effect on kinetic and equilibrium constants

We next sought to gain more information on the nature of the rate-determining step for peptide exchange. We reasoned that decreasing the pH might influence either

the inter-molecular electrostatic interactions such as attraction<sup>36,37</sup> or repulsion of the peptide; this would alter  $k_{\text{on}}$  or  $k_{\text{off}}$ , which we had largely excluded above. Alternatively, a pH decrease might influence MHC-I conformation or conformational dynamics, making the MHC-I molecule more susceptible to peptide binding and thus leading indirectly to a faster binding of peptide. We further reasoned that we might be able to differentiate between these two explanations by using a high salt concentration, since salt disrupts long-range electrostatic ligand-receptor interactions more strongly than it disturbs protein conformational changes.<sup>38,39</sup>

We, thus, repeated the peptide exchange, binding affinity, and association rate determination experiments for dsA2 and dsA24 in the presence of 500 mM NaCl. While the equilibrium binding affinities were generally not affected (Figure S3a,b), the exchange rate of A2 decreased by about factor 10 with high salt, but the pH dependence remained (Figure 3a,b). For A24, the effect of salt was not significant. Interestingly, association rates were also not much affected by high salt (Figure S3c,d), suggesting that in the binding of peptides to A2 and A24, electrostatic attraction of the peptide by the protein does not play a significant role. We conclude that while allotype-specific differences exist, the high-salt experiments give no convincing evidence for an involvement of peptide association or dissociation steps in limiting the

rate of peptide exchange, but instead point to an effect of the pH on the conformation, or the conformational dynamics, of the molecule.

Taken together, the results so far suggest that pH changes do not affect peptide association, peptide dissociation, or equilibrium affinity of peptide binding to an extent large enough to explain the dramatic acceleration of peptide exchange with lower pH that is seen in Figure 1c–f, and that we need to investigate the conformational change of MHC-I itself.

## 2.5 | Evidence for an unstable intermediate

The peptide-empty intermediate of the exchange reaction ( $M_{\text{empty}}$  in Equation 2) is accessible to us in the form of the peptide-free disulfide-stabilized A2 or A24 molecules. We thus measured their thermostabilities by nanoDSF, and we found that both empty dsMHC-I are significantly (10–12°C) stabilized against denaturation by low pH (Figure 4a). We therefore decided to expand our model by assuming that the intermediate of the exchange reaction, that is, the peptide-empty MHC-I, exists in an equilibrium between a native empty form that can rapidly bind peptide ( $M_{\text{receptive}}$ ) and a partially unfolded empty form that does not bind peptide ( $M_{\text{non-receptive}}$ ). Such an

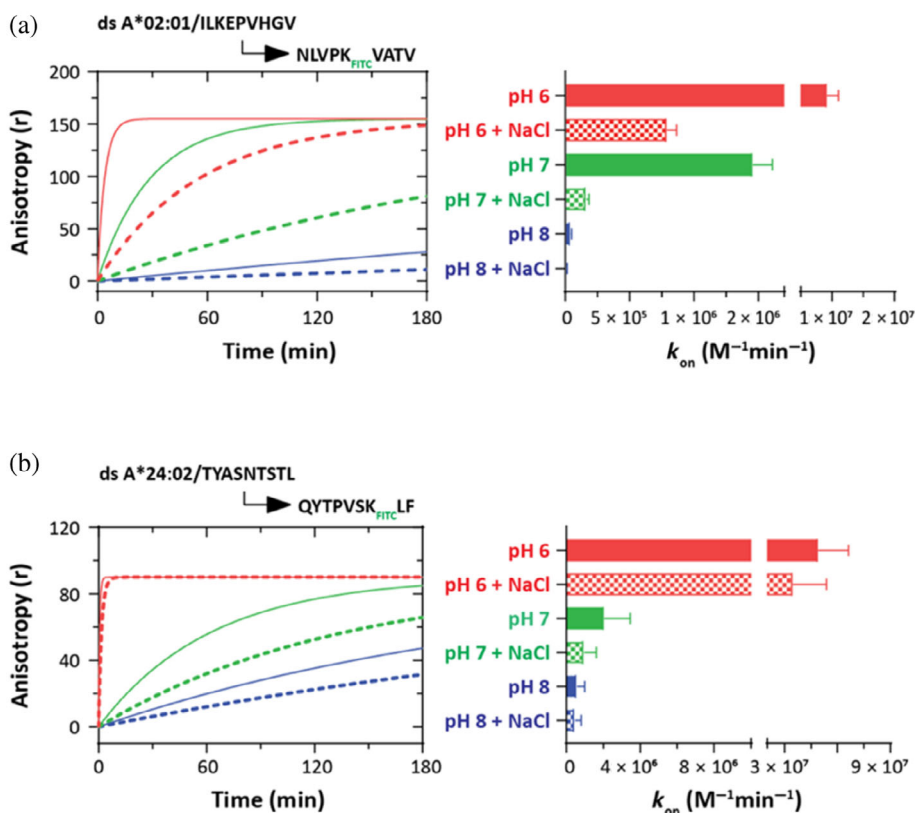


**FIGURE 3** Evidence for long-range peptide-MHC-I interaction with dsA2 but not dsA24. Exchange reaction with 60 nM of the high affinity peptide-MHC-I (a) dsA2/ILKEPVHGV and (b) dsA24/TYASNTSTL with 20 nM incoming FITC peptides in citrate-phosphate buffer at pH 7 and 8, with or without 500 mM NaCl. Values and repeats are in Table S1.

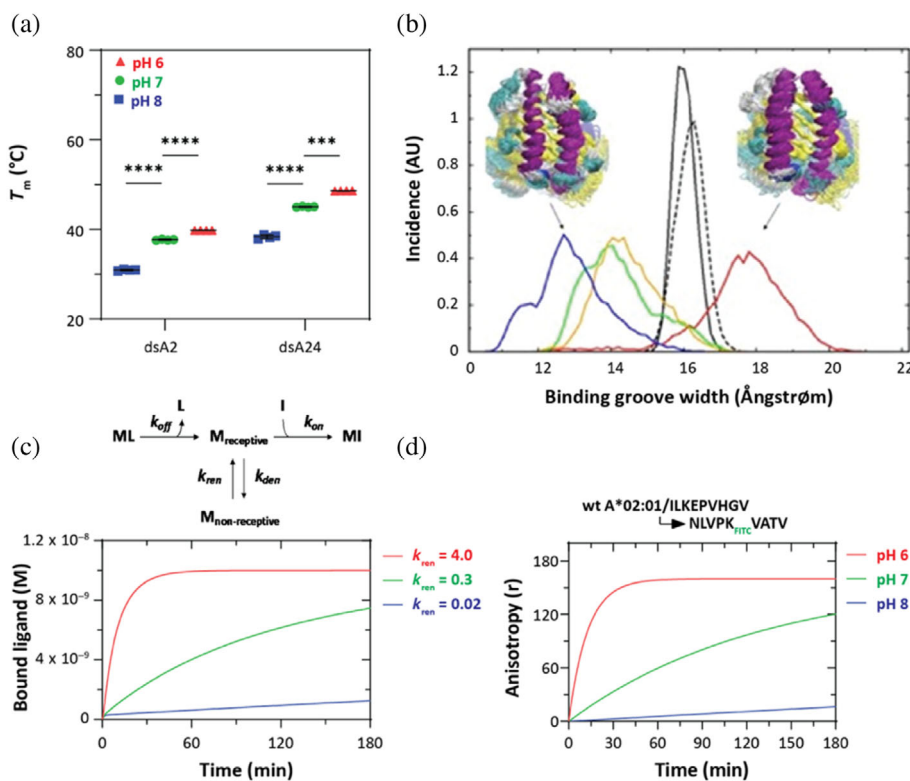
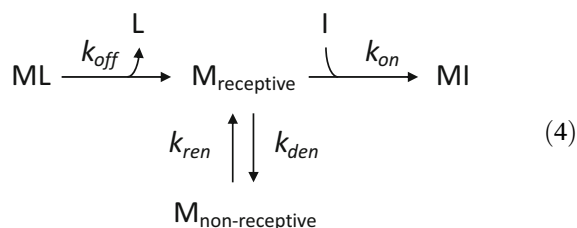


**FIGURE 4** Acidic acceleration of peptide exchange occurs by stabilization of a peptide-empty intermediate. (a) Thermal stability measurement for 2.2  $\mu$ M of empty dsA2 and dsA24 molecules at pH 6, 7, and 8. Values and repeats are in Table S2. (b) Probability distribution of binding cleft size observed during MD simulations of the peptide-bound states (black line: dsA24; dashed black line: dsA2), the empty state of dsA2 (pH 6: red line, pH 8: green line) and empty state of dsA24 (pH 6: orange line, pH 8: blue line). The binding cleft size was measured as center-of-mass distance between residues forming the  $\alpha_1$  (residues 56–85) and  $\alpha_2$  (residues: 138–173) helices. Sampled example structure distributions are indicated for dsA24 at pH 8 (left inset) and dsA2 at pH 6 (right inset). The sampled structure frames were superimposed with respect to residues forming the binding cleft. The color code represents the secondary structure. Snapshots of the MD simulations are in Figure S5. (c) Kinetic simulation of peptide exchange assuming a tendency of the empty intermediate to reversibly unfold (Equation 4 shown above the plot). Simulation parameters are:  $[ML]_{t=0}$ , 30 nM and  $[I]_{t=0}$ , 10 nM (the same values as in the experiment in D);  $k_{off}$ , 1  $\text{min}^{-1}$ ;  $k_{den}$ , 100  $\text{min}^{-1}$ ;  $k_{on}$ ,  $10^8 \text{ M}^{-1} \text{ min}^{-1}$ . Compare with (d), which is identical to Figure 1e

equilibrium has been postulated by us and others<sup>20,32,40,41</sup>:



where  $k_{den}$  and  $k_{ren}$  are the rate constants for the transitions to (den = denaturation) and from (ren = renaturation) the unfolded empty state. We then assumed that the pH influences the  $\text{M}_{\text{folded}} \rightleftharpoons \text{M}_{\text{unfolded}}$  equilibrium such that at pH 6, there is more  $\text{M}_{\text{receptive}}$ , leading to the higher denaturation temperatures seen in Figure 4a. To test this assumption in a mathematical model, we performed a kinetic

simulation of an exchange reaction with all known parameters, and we were able to recapitulate the results of Figure 1e by assuming a tenfold decrease of  $k_{ren}$  between pH 8 and pH 7, and again between pH 7 and pH 6, without assuming any pH-mediated changes to  $k_{on}$  or  $k_{off}$  (Figure 4c,d). We conclude that the simplest applicable model predicts a pH-dependent reversible equilibrium between two states of the peptide-empty intermediate of the exchange reaction.

To model the dynamic behavior of A2 and A24 during the intermediate unbound state, we performed molecular dynamics (MD) simulations, using as start structures published crystal structures with the bound peptide coordinates removed. To mimic the dominant protonation states, the ionizable side chains located in the binding groove were assumed to be protonated at pH 6 (Glu55, Glu63, Asp77, His70, His74, and His114 residues in HLA-A\*02:01 vs. Glu55, Glu63, Asp74, His70 and His74 in

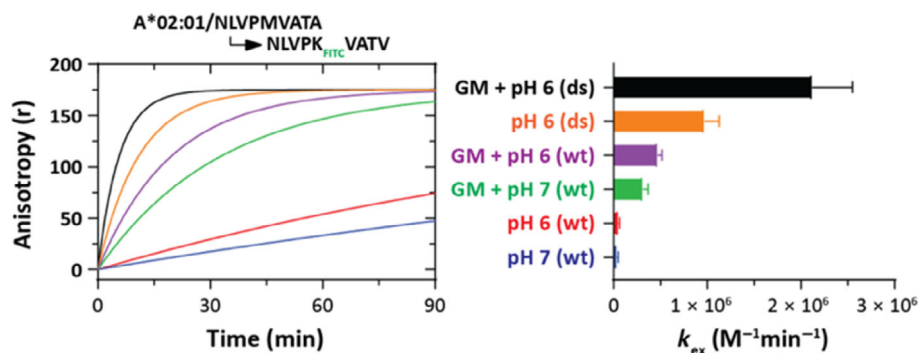


**FIGURE 5** Synergy between disulfide stabilization, dipeptides, and low pH in peptide exchange. Exchange reaction with 60 nM of the low affinity peptide-MHC-I complexes of wtA2- and dsA2-NLVPMVATA with 20 nM incoming FITC labelled peptide in citrate-phosphate buffer at pH 6 and 7, with or without 10 mM GM and respective exchange rate constant ( $k_{ex}$ ) values on right. Values and repeats are in Table S1.

HLA-A\*24:02) and adopting the standard ionization states at pH 8 (acidic residues charged, histidine neutral), which represents the extremes of possible protonation states of residues in the binding groove at the two pH values. During the simulations (up to 750 ns), the  $\alpha_1$  and  $\alpha_2$  helices that form the peptide binding groove exhibited enhanced fluctuations compared to the simulations in the presence of bound peptide at both pH values. No unfolding of the structures was observed. However, at pH 6, both allotypes adopted more open grooves than at pH 8 (Figure 4b). In the closed forms seen at pH 8, the binding grooves are too narrow to accommodate an incoming peptide, whereas open states with a groove that is wider, or closer to the bound state, may still allow productive peptide binding. Hence, the MD simulations suggest that the non-receptive empty form may correspond to a structure with a closed binding groove that needs to re-open in order to bind the peptide. The dominance of the closed state observed in the MD simulations at pH 8 explains the dramatic reduction of the peptide exchange at pH 8 vs. pH 6.

## 2.6 | Acidic acceleration is synergistic with dipeptide-mediated peptide exchange

Finally, we put this model to the test by examining its synergy with dipeptide-mediated peptide exchange. We previously demonstrated that dipeptides of appropriate sequence accelerate peptide dissociation ( $k_{off}$ , by displacing the termini of the peptide,<sup>11</sup>) and association ( $k_{on}$ , by keeping the F pocket region in a folded state<sup>42</sup>). We reasoned that if low pH accelerated exchange by a different mechanism, for example, conformational stabilization of the intermediate, then the two should be strongly synergistic. Indeed, when comparing the effect of pH and

dipeptide on peptide exchange for wtA2, we found that they synergized in accelerating peptide exchange (Figure 5). We conclude that the data are consistent with a model in which dipeptides and low pH accelerate peptide exchange by separate mechanisms.

## 3 | DISCUSSION

The kinetics of peptide binding and exchange are central to the dynamic process of peptide selection and optimization in live cells, which co-determines immunodominance and is thus essential to vaccine design.<sup>25,33,43–46</sup> Peptide exchange is especially interesting in cross-presentation, where professional antigen-presenting cells present exogenous peptides on MHC-I<sup>6,47,48</sup>; this process may not rely on peptide-empty MHC-I molecules escaping from the ER but involve the exchange of ER-bound peptides for peptides generated from endocytosed material in the endosomes.<sup>15,48–51</sup> Since ER-loaded and tapasin-optimized peptide/MHC-I complexes are stable on the timescale of minutes to hours, researchers have asked whether the acid environment of endosomes might accelerate the peptide exchange for crosspresentation.<sup>6,7,15,49</sup> We show here that at pH 6, peptide exchange on A2 and A24 is indeed significantly accelerated.

Peptide association kinetics has been especially difficult to study, since the empty forms of class I that were available had slow binding kinetics and are assumed to be in a molten globule state.<sup>20,32,52,53</sup> The advent of disulfide-stabilized empty molecules has made such association studies possible.<sup>8</sup> Thus, we have been able to test the recent proposition—from MD simulations—that peptide binding to A24 is strongly supported by electrostatic attraction<sup>54</sup>; this is not supported by our data, which show only a mild decrease in the association rate at high

salt for A2, and none for A24. So, while binding (and dissociation) kinetics of peptides to MHC-I are allotype-specific in detail, we do not find evidence for long-range interactions between receptor and ligand in the association process.

This also means that the acidic acceleration of peptide exchange that we describe here is not caused by an electrostatic charge that would attract the peptide. Likewise, we exclude effects on peptide dissociation and on the equilibrium constant. This leaves as the simplest explanation a model of a peptide-empty intermediate of the reaction that exists in two states, only one of which is peptide-receptive, and whose equilibrium is shifted with changing pH (Equation 4).

Such an unstable empty intermediate is not a leap of faith. Peptide-empty class I molecules were always known to be conformationally unstable, both in vitro and in cells,<sup>40,55</sup> and this showed in MD simulations.<sup>25,41,56</sup> From such simulations, we can assume that there are not two empty forms but an ensemble or continuum of many states; but a simulation with two states already gives sufficient approximation to the data (Figure 4c). A calculation demonstrates that there is enough time during an exchange reaction for an MHC-I protein to partially unfold: a typical association rate of 10 nM peptide to dsA2 is  $2 \times 10^7 \text{ M}^{-1} \text{ min}^{-1}$  (Figure 2a), giving a collision frequency of  $0.2 \text{ min}^{-1}$  and a half-time of 3.5 min for the productive binding of exogenous peptide to empty A2. Thus, during an exchange reaction, the binding site may remain empty for several minutes until an incoming peptide molecule binds productively. The model in Equation 4 assumes that at acidic pH, a larger proportion of the peptide-free intermediate of the exchange reaction is in a peptide-receptive state ( $M_{\text{receptive}}$ ) than at neutral pH. This is strongly supported by our finding that if the pH is lowered, the  $k_{\text{ex}}$  increases until it comes close to the  $k_{\text{on}}$ , suggesting that a substantial portion, if not all, of MHC-I molecules is available for productive peptide binding (Figure S4), that is, that peptide dissociation is not a rate-limiting step, and that  $M_{\text{receptive}} \gg M_{\text{non-receptive}}$  at pH 6.

Why, then, are the  $k_{\text{on}}$  values at pH 8 and pH 6 barely different from each other? This apparent paradox is explained by a thought experiment: in fluorescence anisotropy, the fastest association rate will always dominate the initial rate determination, and so one always measures the  $k_{\text{on}}$  to the  $M_{\text{receptive}}$  if it is present in the mixture.

For us, the structure of the  $M_{\text{receptive}}$  and  $M_{\text{non-receptive}}$  states is especially interesting. We and others have found that in empty MHC-I, the F pocket region is especially conformationally flexible.<sup>25,40,41,56,57</sup> When the two helices are covalently connected with a disulfide bond between residues 84 and 139, conformational fluctuations

decrease (as proposed by MD simulations), and recombinant MHC-I remain soluble in their peptide-free form, suggesting that F pocket conformational stabilization is a main task of the bound peptide in maintaining MHC-I stability.<sup>8,28</sup> The substantial increase of  $k_{\text{on}}$  and  $k_{\text{ex}}$  that we observe with dsMHC-I over wtMHC-I (Table S1) thus formally demonstrates that conformational stabilization of a peptide-free intermediate accelerates peptide association. However, acidic acceleration is not identical to disulfide stabilization. We know that because low pH leads to a considerable  $k_{\text{ex}}$  increase even for the dsMHC-I (Figure S1e,f). Importantly, this mechanistic difference also applies to the wtMHC-I (i.e., it is not an artifact of the dsMHC-I proteins), since low pH and dipeptides (which stabilize the F pocket like the disulfide bond,<sup>11,27,28</sup>) are synergistic in exchange acceleration (Figure 5). The observation that disulfide stabilization does not work for all MHC-I allotypes (S. Sp., unpublished) agrees with this observation, further suggesting that other regions of MHC-I may need to be stabilized. Still, after all, we do not yet know which exact conformational rearrangement accompanies the  $M_{\text{receptive}} \rightleftharpoons M_{\text{non-receptive}}$  transition of Equation 4. It might be one of the movements of the binding site observed previously,<sup>19</sup> or else it might involve a movement of the  $\alpha_1/\alpha_2$  domain relative to the  $\alpha_3$  domain, or to  $\beta_2\text{m}$ .

The maximal peptide exchange rate that can be achieved at low pH is tenfold higher for A24 than for A2 (Table S1). According to our data, the simplest explanation is that the peptide-free intermediate of A24 is proportionally more in the  $M_{\text{receptive}}$  state. This explanation is supported by our observation that the peptide-empty form of A24 has a much higher  $T_m$  ( $\Delta T_m = 7.5^\circ\text{C}$  at pH 8) than empty A2 (Figure 4a). We have shown earlier that MHC-I allotypes differ in the conformational stability of the empty form, and that this correlates with dependence on the conformational chaperone, tapasin.<sup>19,40,56</sup> However, A2 and A24 share a low tapasin dependence,<sup>58</sup> which suggests that the response of empty MHC-I to acidic conditions, as encountered in the endosomes, is governed by a set of rules that are as yet unknown. It will be exciting to uncover them, and to correlate them with cross-presentation in living cells, where the low pH of endosomes is known to be very important for the recycling of endocytosed MHC-I to the surface.<sup>59</sup>

## 4 | METHODS

### 4.1 | Production of MHC-I heavy chains and $\beta_2\text{m}$

MHC-I heavy chains and  $\beta_2\text{m}$  were produced in *E. coli*, as described previously.<sup>20,60</sup> Briefly, proteins were



expressed in *BL21(DE3)pLysS* using pET series plasmids (Novagen). Inclusion bodies containing expressed proteins were harvested by sonication in lysis buffer followed by washing in detergent buffer and wash buffer and solubilizing the protein in 8 M urea buffer (8 M urea, 50 mM HEPES pH 6.5, and 100  $\mu$ M  $\beta$ -mercaptoethanol). Proteins were stored at  $-80^{\circ}\text{C}$  until used for in vitro folding.

## 4.2 | In-vitro folding and purification of MHC-I

All MHC-I proteins were folded and purified as previously described.<sup>8</sup> Briefly, wtA2, dsA2, wtA24 and dsA24 molecules, heavy chains (1  $\mu$ M) and  $\beta_2\text{m}$  (2  $\mu$ M) diluted in a folding buffer composed of 0.1 M Tris pH 8.0, 500 mM L-Arginine-HCl, 2 mM EDTA, 0.5 mM oxidized glutathione and 5 mM reduced glutathione with 10  $\mu$ M low-affinity peptides or with 10 mM of dipeptide (GM for A2, GF for A24). The folding reaction was then incubated at  $4^{\circ}\text{C}$  for 1 week, followed by concentrating folded proteins with a 30 kDa cutoff membrane filters (Vivaflow-200; Sartorius). Folded MHC-I monomers were purified with size exclusion chromatography using ÄKTA Go HiLoad 26/600 Superdex-200 pg gel filtration column (Cytiva). All MHC-I folded monomers were stored at  $-80^{\circ}\text{C}$  until further use.

## 4.3 | Thermal stability measurements

Thermal stability was measured using nanoDSF by dissolving MHC-I complexes in citrate-phosphate buffer, pH 7.6<sup>61</sup> at the concentration of 100  $\mu\text{g}/\text{ml}$ . Each capillary was loaded with 10  $\mu\text{l}$  of test samples either in duplicates or triplicates. Experiments were carried out using the Prometheus NT.48 (Nano Temper Technologies). The temperature gradient was set to an increase of  $1^{\circ}\text{C}/\text{min}$  in a range from 20 to  $80^{\circ}\text{C}$ .  $T_m$  values were calculated by the PR. ThermControl v2.1 software from the first derivative of the fluorescence at F330 and plotted using GraphPad prism.

## 4.4 | Peptide binding, exchange, and dissociation

Peptide binding and exchange was performed using fluorescence anisotropy as previously described.<sup>8,11,42</sup> To assess peptide binding by fluorescence anisotropy, 10 nM fluorochrome-labeled peptide NLVPK<sub>FITC</sub>VATV or QYTPVSK<sub>FITC</sub>LF (GeneCust) and 30 nM of purified

folded empty dsA2 or dsA24 were used unless otherwise mentioned. The FITC subscript denotes the lysine residue whose side chain was modified with fluorescein, taking care that labeling the peptide did not interfere with binding to MHC-I. Peptide binding was measured at room temperature ( $22\text{--}24^{\circ}\text{C}$ ) in citrate-phosphate buffer pH 6, pH 7, and pH 8 in a total reaction volume of 100  $\mu\text{l}$ .

For peptide exchange studies, 10 nM of NLVPK<sub>FITC</sub>VATV or QYTPVSK<sub>FITC</sub>LF (GeneCust) was added to 30 nM of purified MHC-I/peptide complexes of wt or dsA2 or A24, respectively. Where indicated, the dipeptides GM, GL and GF (in the single-letter amino acid code; by GeneCust) were added at 10 mM final concentration.

For peptide dissociation studies, 10 nM of NLVPK<sub>TAM-RA</sub>VATA was added to 30 nM of purified empty dsA2, followed by the addition of 10  $\mu\text{M}$  NLVPMVATV after 1 hr. Association was tracked for the first hour, followed by dissociation for 6 hr following addition of NLVPMVATV.

All kinetic measurements were performed with Tecan Infinite M1000 PRO (Tecan) multimode plate reader by measuring anisotropy (FITC  $\lambda_{\text{ex}} = 494$  nm,  $\lambda_{\text{em}} = 517$  nm). Data were plotted using GraphPad Prism.

## 4.5 | Kinetics simulations

Kinetics simulations were done in Microsoft Excel with 10,800 steps and a time increment of 1 s.

## 4.6 | Molecular dynamics simulations

MD simulations were performed starting from the coordinates of A2 (pdb entry pdb5d2n) and A24 (pdb entry pdb2bck). For the simulations in the absence of bound peptides, the coordinates of the bound peptides were removed. The disulfide bridge to generate the disulfide-stabilized variants was introduced by in silico substitution of residues 84 and 139 by Cys residues. Protonation states of acidic and basic groups were calculated using the H++ server (Gordon et al., 2005). To mimic the upper and lower bounds of protonation states of ionizable residues buried in the binding cleft, the Glu55, Glu63, Asp77, His70, His74, and His114 residues in A2 and the Glu55, Glu63, Asp74, His70, and His74 in A24 were assumed to be protonated at pH 6 (standard protonation states at pH 8). All simulations were performed using the Amber18 package.<sup>62</sup> Proteins were solvated in octahedral boxes with explicit TIP3P water molecules<sup>63</sup> keeping a minimum distance of 10  $\text{\AA}$  between protein atoms and box boundaries. The ion concentration was adjusted to 0.1 M with explicit sodium and chloride ions. The parm14SB force field was used for the proteins and

peptides.<sup>64</sup> The simulation systems were energy minimized (5,000 steps) after solvation followed by heating up to 310 K in steps of 100 K with position restraints on all heavy atoms of the proteins. Subsequently, positional restraints were gradually removed from an initial 12 kcal·mol<sup>-1</sup>·Å<sup>-2</sup> to 0.5 kcal·mol<sup>-1</sup>·Å<sup>-2</sup> within 0.5 ns followed by a 1 ns unrestrained equilibration at 310 K. All production simulations were performed at a temperature of 310 K and a pressure of 1 bar. The hydrogen mass repartition option of Amber was used to allow a time step of 4 fs.<sup>65</sup> Unrestrained production simulations for up to 750 ns were performed. Trajectory analysis was performed using the cpptraj module of the Amber18 package.

## AUTHOR CONTRIBUTIONS

**Ankur Saikia:** Conceptualization (equal); data curation (lead); formal analysis (lead); investigation (lead); methodology (lead); validation (lead); writing – original draft (equal). **Andries Haderer:** Data curation (supporting); formal analysis (supporting); investigation (supporting). **Pranathi Prasad:** Formal analysis (supporting); writing – original draft (equal). **Martin Zacharias:** Data curation (supporting); formal analysis (supporting); investigation (supporting); software (lead); visualization (lead); writing – review and editing (supporting). **Sebastian Springer:** Conceptualization (equal); project administration (lead); resources (lead); supervision (lead); validation (supporting); writing – original draft (supporting); writing – review and editing (lead).

## ACKNOWLEDGMENTS

The authors thank Uschi Wellbrock for excellent technical support. We acknowledge funding from the Deutsche Forschungsgemeinschaft (SP583/12-1 to Sebastian Springer).

## CONFLICT OF INTEREST


The authors declare that no competing interests exist.

## DATA AVAILABILITY STATEMENT

Data available on request from the authors.

## ORCID

Ankur Saikia  <https://orcid.org/0000-0002-7169-5765>

Sebastian Springer  <https://orcid.org/0000-0002-5527-6149>

## REFERENCES

- Paul WE. Fundamental immunology. Philadelphia, PA, USA: Wolters Kluwer Health/Lippincott Williams & Wilkins, 2013.
- Elliott T, Williams A. The optimization of peptide cargo bound to MHC class I molecules by the peptide-loading complex. *Immunol Rev*. 2005;207:89–99.
- Thomas C, Tampé R. MHC I assembly and peptide editing - chaperones, clients, and molecular plasticity in immunity. *Curr Opin Immunol*. 2021;70:48–56.
- Praveen PVK, Yaneva R, Kalbacher H, Springer S. Tapasin edits peptides on MHC class I molecules by accelerating peptide exchange. *Eur J Immunol*. 2010;40:214–224.
- Ackerman AL, Cresswell P. Cellular mechanisms governing cross-presentation of exogenous antigens. *Nat Immunol*. 2004; 5:678–684.
- Chefalo PJ, Harding CV. Processing of exogenous antigens for presentation by class I MHC molecules involves post-Golgi peptide exchange influenced by peptide-MHC complex stability and acidic pH. *J Immunol*. 2001;167:1274–1282.
- Stryhn A, Pedersen LO, Romme T, et al. pH dependence of MHC class I-restricted peptide presentation. *J Immunol*. 1996; 156:4191–4197.
- Saini SK, Tamhane T, Anjanappa R, et al. Empty peptide-receptive MHC class I molecules for efficient detection of antigen-specific T cells. *Sci Immunol*. 2019;4:eaau9039.
- Moritz A, Anjanappa R, Wagner C, et al. High-throughput peptide-MHC complex generation and kinetic screenings of TCRs with peptide-receptive HLA-A\*02:01 molecules. *Sci Immunol*. 2019;4:eaav0860.
- Luimstra JJ, Garstka MA, Roex MCJ, et al. A flexible MHC class I multimer loading system for large-scale detection of antigen-specific T cells. *J Exp Med*. 2018;215:1493–1504.
- Saini SK, Schuster H, Ramnarayan VR, Rammensee HG, Stevanović S, Springer S. Dipeptides catalyze rapid peptide exchange on MHC class I molecules. *Proc Natl Acad Sci U S A*. 2015;112:202–207.
- Rodenko B, Toebes M, Hadrup SR, et al. Generation of peptide-MHC class I complexes through UV-mediated ligand exchange. *Nat Protoc*. 2006;1:1120–1132.
- Rodenko B, Toebes M, Celie P, Perrakis A, Schumacher TNM. MHC class I complexes loaded by a periodate trigger. *Water*. 2013;131:1–10.
- Overall SA, Toor JS, Hao S, et al. High throughput pMHC-I tetramer library production using chaperone-mediated peptide exchange. *Nat Commun*. 2020;11:1909.
- Grommé M, Uytdehaag FGCM, Janssen H, et al. Recycling MHC class I molecules and endosomal peptide loading. *Proc Natl Acad Sci U S A*. 1999;96:10326–10331.
- Garboczi DN, Hung DT, Wiley DC. HLA-A2-peptide complexes: Refolding and crystallization of molecules expressed in *Escherichia coli* and complexed with single antigenic peptides. *Proc Natl Acad Sci U S A*. 1992;89:3429–3433.
- Saikia A, Springer S. Peptide-MHC I complex stability measured by nanoscale differential scanning fluorimetry reveals molecular mechanism of thermal denaturation. *Mol Immunol*. 2021;136:73–81.
- Hochman JH, Jiang H, Matyus L, Edidin M, Pernis B. Endocytosis and dissociation of class I MHC molecules labeled with fluorescent beta-2 microglobulin. *J Immunol*. 1991;146:1862–1867.
- Jantz-Naeem N, Springer S. Venus flytrap or pas de trois? The dynamics of MHC class I molecules. *Curr Opin Immunol*. 2021;70:82–89.
- Saini SK, Abualrous ET, Tigan AS, Covella K, Wellbrock U, Springer S. Not all empty MHC class I molecules are molten globules: Tryptophan fluorescence reveals a two-step mechanism of thermal denaturation. *Mol Immunol*. 2013;54:386–396.

21. Arosa FA, Esgalhado AJ, Reste-Ferreira D, Cardoso EM. Open MHC class I conformers: A look through the looking glass. *Int J Mol Sci.* 2021;22:9738.
22. Truong HV, Sgourakis NG. Dynamics of MHC-I molecules in the antigen processing and presentation pathway. *Curr Opin Immunol.* 2021;70:122–128.
23. Natarajan K, Jiang J, May NA, et al. The role of molecular flexibility in antigen presentation and T cell receptor-mediated signaling. *Front Immunol.* 2018;9:1657.
24. van Hateren A, Bailey A, Werner JM, Elliott T. Plasticity of empty major histocompatibility complex class I molecules determines peptide-selector function. *Mol Immunol.* 2015;68:98–101. <https://doi.org/10.1016/j.molimm.2015.03.010>.
25. Wieczorek M, Abualrous ET, Sticht J, et al. Major histocompatibility complex (MHC) class I and MHC class II proteins: Conformational plasticity in antigen presentation. *Front Immunol.* 2017;8:1–16.
26. Hein Z, Uchtenhagen H, Abualrous ET, et al. Peptide-independent stabilization of MHC class I molecules breaches cellular quality control. *J Cell Sci.* 2014;127:2885–2897.
27. Hafstrand I, Sayitoglu EC, Apavaloaei A, et al. Successive crystal structure snapshots suggest the basis for MHC class I peptide loading and editing by tapasin. *Proc Natl Acad Sci U S A.* 2019;116:5055–5060. <https://doi.org/10.1073/pnas.1807656116>.
28. Anjanappa R, Garcia-Alai M, Kopicki JD, et al. Structures of peptide-free and partially loaded MHC class I molecules reveal mechanisms of peptide selection. *Nat Commun.* 2020;11:1–11.
29. Swonger KN, Robinson AS. Using fluorescence anisotropy for ligand binding kinetics of membrane proteins. *Curr Protoc Protein Sci.* 2018;93:e63.
30. Springer S, Do K, Skipper JCA, Townsend ARM, Cerundolo V. Fast association rates suggest a conformational change in the MHC class I molecule H-2Db upon peptide binding. *Biochemistry.* 1998;2960:3001–3012.
31. Kopicki J-D, Saikia A, Niebling S, et al. Opening opportunities for Kd determination and screening of MHC peptide complexes. *Commun Biol.* 2022;5:488.
32. Bouvier M, Wiley DC. Structural characterization of a soluble and partially folded class I major histocompatibility heavy chain/ $\beta$ 2m heterodimer. *Nat Struct Biol.* 1998;5:377–384.
33. Fahnstock ML, Johnson JL, Feldman RMR, et al. Effects of peptide length and composition on binding to an empty class I MHC heterodimer. *Biochemistry.* 1994;33:8149–8158.
34. Hulsmeyer M, Welfle K, Pöhlmann T, et al. Thermodynamic and structural equivalence of two HLA-B27 subtypes complexed with a self-peptide. *J Mol Biol.* 2005;346:1367–1379.
35. Hellman LM, Yin L, Wang Y, et al. Differential scanning fluorimetry based assessments of the thermal and kinetic stability of peptide-MHC complexes. *J Immunol Methods.* 2016;432:95–101.
36. Leckband DE, Israelachvili JN, Schmitt F-J, Knoll W. Long-range attraction and molecular rearrangements in receptor-ligand interactions. *Science.* 1992;255:1419–1421.
37. Sharp K, Fine R, Honig B. Computer simulations of the diffusion of a substrate to an active site of an enzyme. *Science.* 1987;236:1460–1463.
38. Tsumoto K, Ejima D, Senczuk AM, Kita Y, Arakawa T. Effects of salts on protein-surface interactions: Applications for column chromatography. *J Pharm Sci.* 2007;96:1677–1690.
39. Darling RJ, Kuchibhotla U, Glaesner W, Micanovic R, Witcher DR, Beals JM. Glycosylation of erythropoietin affects receptor binding kinetics: Role of electrostatic interactions. *Biochemistry.* 2002;41:14524–14531.
40. Garstka MA, Fritzsche S, Lenart I, et al. Tapasin dependence of major histocompatibility complex class I molecules correlates with their conformational flexibility. *FASEB J.* 2011;25:3989–3998.
41. Zacharias M, Springer S. Conformational flexibility of the MHC class I alpha1-alpha2 domain in peptide bound and free states: A molecular dynamics simulation study. *Biophys J.* 2004;87:2203–2214.
42. Saini SK, Ostermeir K, Ramnarayan VR, Schuster H, Zacharias M, Springer S. Dipeptides promote folding and peptide binding of MHC class I molecules. *Proc Natl Acad Sci U S A.* 2013;110:15383–15388.
43. Townsend A, Elliott T, Cerundolo V, Foster L, Barber B, Tse A. Assembly of MHC class I molecules analyzed in vitro. *Cell.* 1990;62:285–295.
44. Chen W, McCluskey J. Immunodominance and immunodominance: Critical factors in developing effective CD8+ T-cell-based cancer vaccines. *Adv Cancer Res.* 2006;95:203–247.
45. Yewdell JW. Confronting complexity: Real-world immunodominance in antiviral CD8+ T cell responses. *Immunity.* 2006;25:533–543.
46. Wellington D, Yin Z, Kessler BM, Dong T. Immunodominance complexity: Lessons yet to be learned from dominant T cell responses to SARS-COV-2. *Curr Opin Virol.* 2021;50:183–191.
47. Kovacovics-Bankowski M, Rock K. A phagosome-to-cytosol pathway for exogenous antigens presented on MHC class I molecules. *Science.* 1995;267:243–246.
48. Schirmbeck R, Melber K, Reimann J. Hepatitis B virus small surface antigen particles are processed in a novel endosomal pathway for major histocompatibility complex class I-restricted epitope presentation. *Eur J Immunol.* 1995;25:1063–1070.
49. Montealegre S, van Endert PM. Endocytic recycling of MHC class I molecules in non-professional antigen presenting and dendritic cells. *Front Immunol.* 2019;9:3098.
50. Basha G, Lizée G, Reinicke AT, Seipp RP, Omilusik KD, Jefferies WA. MHC class I endosomal and lysosomal trafficking coincides with exogenous antigen loading in dendritic cells. *PLoS ONE.* 2008;3:e3247.
51. Mahmutefendic H, Blagojevic G, Tomas MI, Kucic N, Lucin P. Segregation of open major histocompatibility class I conformers at the plasma membrane and during endosomal trafficking reveals conformation-based sorting in the endosomal system. *Int J Biochem Cell Biol.* 2011;43:504–515.
52. Olsen AC, Pedersen LØS, Hansen AS, et al. A quantitative assay to measure the interaction between immunogenic peptides and purified class I major histocompatibility complex molecules. *Eur J Immunol.* 1994;24:385–392.
53. Ljunggren HG, Stam NJ, Öhlén C, et al. Empty MHC class I molecules come out in the cold. *Nature.* 1990;346:476–480.
54. Bekker G-J, Kamiya N. N-terminal-driven binding mechanism of an antigen peptide to human leukocyte antigen-a\*2402 elucidated by multicanonical molecular dynamic-based dynamic docking and path sampling simulations. *J Phys Chem B.* 2021;125:13376–13384.
55. Kienast A, Preuss M, Winkler M, Dick TP. Redox regulation of peptide receptivity of major histocompatibility complex class I molecules by ERp57 and tapasin. *Nat Immunol.* 2007;8:864–872.

56. Abualrous ET, Fritzsche S, Hein Z, et al. F pocket flexibility influences the tapasin dependence of two differentially disease-associated MHC class I proteins. *Eur J Immunol*. 2015;45:1248–1257.
57. Narzi D, Becker CM, Fiorillo MT, Uchanska-Ziegler B, Ziegler A, Böckmann RA. Dynamical characterization of two differentially disease associated MHC class I proteins in complex with viral and self-peptides. *J Mol Biol*. 2012;415:429–442.
58. Bashirova AA, Viard M, Naranbhai V, et al. HLA tapasin independence: Broader peptide repertoire and HIV control. *Proc Natl Acad Sci U S A*. 2020;117:28232–28238.
59. Reid PA, Watts C. Cycling of cell-surface MHC glycoproteins through primaquine-sensitive intracellular compartments. *Nature*. 1990;346:655–657.
60. Garboczi DN, Hung DT, Wiley DONC. PNAS-1992-Garboczi-3429-33. *Proc Natl Acad Sci U S A*. 1992;89:3429–3433.
61. McIlvaine TC. A buffer solution for colorimetric comparison. *J Biol Chem*. 1921;49:183–186.
62. Case D, Ben-Shalom I, Brozell SR, et al. AMBER 2018. San Francisco, CA, 2018.
63. Jorgensen WL, Chandrasekhar J, Madura JD, Impey RW, Klein ML. Comparison of simple potential functions for simulating liquid water. *J Chem Phys*. 1983;79:926–935.
64. Maier JA, Martinez C, Kasavajhala K, Wickstrom L, Hauser KE, Simmerling C. ff14SB: Improving the accuracy of protein side chain and backbone parameters from ff99SB. *J Chem Theory Comput*. 2015;11:3696–3713.
65. Hopkins CW, Le Grand S, Walker RC, Roitberg AE. Long-time-step molecular dynamics through hydrogen mass repartitioning. *J Chem Theory Comput*. 2015;11:1864–1874.

## SUPPORTING INFORMATION

Additional supporting information can be found online in the Supporting Information section at the end of this article.

**How to cite this article:** Saikia A, Hadelers A, Prasad P, Zacharias M, Springer S. Fast peptide exchange on major histocompatibility complex class I molecules by acidic stabilization of a peptide-empty intermediate. *Protein Science*. 2022; 31(12):e4478. <https://doi.org/10.1002/pro.4478>